Structure characteristics of nanocrystalline element selenium with different grain sizes

Y. H. Zhao, K. Zhang, and K. Lu*
State Key Laboratory for RSA, Institute of Metal Research, Chinese Academy of Sciences, Shenyang 110015, People's Republic of China
(Received 4 February 1997; revised manuscript received 23 April 1997)

Porosity-free nanocrystalline (nc) element Se samples with mean grain sizes ranging from 13 to 70 nm were synthesized by crystallizing a melt-quenched amorphous Se solid. Microstructures of the nc-Se (with a hcp structure) samples were characterized by means of quantitative x-ray-diffraction measurements. The Bragg reflection and the background intensities, as well as the reflection shape of the x-ray-diffraction patterns for the nc Se were analyzed according to data fitting of the measurement results. The grain-size dependencies of the microstrain, lattice parameters, unit-cell volume, and the mean Debye-Waller parameter were determined. With a reduction of grain size, the microstrain increases significantly along ⟨100⟩ direction but decreases along ⟨104⟩ direction, and exhibits an increasing anisotropic microstrain behavior. The lattice parameter a was found to increase evidently while c decreased slightly with a decreasing grain size, resulting in a significant lattice distortion with a dilated unit-cell volume. It agrees with the observation that the mean Debye-Waller parameter increases with a reduction of grain size, suggesting larger displacements of atoms from their ideal lattice sites in the nc-Se samples with smaller grains. The similarity of the grain-size dependencies of these structural parameters as that of the grain-boundary volume fraction implies that the intrinsic microstructure feature of nc materials is closely related to the crystallite dimension and the amount of grain boundaries. [S0163-1829(97)07245-7]

I. INTRODUCTION

Nanocrystalline (nc) materials are structurally characterized by ultrafine grains and a large number of metastable grain boundaries. Properties of nc materials have been found to be more or less altered, depending upon processing and thermal history of the samples, compared to those of the conventional coarse-grained counterparts.[1–3] A complete characterization of the microstructure of nc materials is necessary for gaining an understanding of the origin of these altered properties in this class of materials.

Quantitative x-ray diffraction (XRD) has been proved to be a powerful tool for structure characterization of nc materials. Previous investigations on nc cubic metals Pd (Ref. 4) (fcc) and Cr (Ref. 5) (bcc) consolidated from ultrafine metallic powders (UFPs), and the nc Cu (fcc) made by means of the severe plastic deformation,[6] etc., have demonstrated that their XRD patterns differ significantly from those of the corresponding reference coarse-grained polycrystalline counterparts. Different structure parameters (such as the microstrain, Debye-Waller parameter, lattice parameter, etc.) have been obtained in the nc materials compared with those for the conventional coarse-grained polycrystalline materials.

Consolidation of UFPs under an ultrahigh pressure (usually greater than 1 GPa) during the synthesis process of the nc compact may introduce a large stress and nanometer-sized pores (or voids) in the sample, which may significantly affect the structure parameters and properties as well. The severe plastic deformation[7] results in bulk porosity-free nc materials (actually the grain size is in the submicron regime), but an evident texture and residual stress are created in the sample that are obstacles for gaining the intrinsic structure feature of nc samples from the XRD data. Nanocrystallization of amorphous solids provides an effective approach to produce porosity-free nc materials.[8,9] During crystallization of the amorphous solid, nanometer-sized crystallites are formed via numerous nucleation and subsequent growth with a controlled rate in the amorphous matrix, eventually resulting in a porosity-free nc sample with a narrow grain-size distribution.[9] The grain size in the as-crystallized sample could be easily changed within a wide range by adjusting the annealing conditions (i.e., varying the nucleation and growth rate), which facilitates the investigation of the grain-size dependence of properties and structure parameters.

In this work, we report a quantitative XRD investigation on the microstructure of porosity-free nc element selenium bulk samples with grain sizes ranging from 13 to 70 nm, which has a different crystallographic symmetry (hcp) compared with other cubic (fcc and bcc) systems. The nc-Se samples were synthesized by means of the complete crystallization of the amorphous solid.[8] The Bragg reflection and the background intensities, as well as the reflection shape of the XRD patterns for the nc Se, were analyzed. Grain-size dependencies of some structure parameters (such as microstrain, lattice parameters, and Debye-Waller parameter, etc.) were determined and analyzed. In addition, low-temperature XRD measurements were performed to study the thermal properties and their grain-size dependencies in this material, which will be addressed in our forthcoming paper.[10] These results will provide an overall picture of the microstructure characteristics of the nc Se and are helpful for understanding the observed properties and structure-property relationship in nc materials.

II. EXPERIMENTAL PROCEDURES

A. Sample preparation

The nanocrystalline selenium specimens in the present work were synthesized by completely crystallizing a melt-

TABLE I. A list of the annealing temperature and the resultant mean grain size in the as-crystallized nc-Se samples. The mean grain size was derived from XRD experiments and verified by TEM observations (in the dark field images).

Annealing temperature (K)	363	371	403	423	433	470	482
Mean grain size, D (nm)	13 ± 2	15 ± 1	23 ± 2	31 ± 3	38 ± 4	60 ± 6	70 ± 5

quenched amorphous selenium solid. Commercial amorphous Se with a purity of 99.999% was sealed in a quartz ampoule with a diameter of 10 mm and a length of 200 mm that was evacuated to 10^{-5} Torr. The solid Se sample was heated to 673 K and held for 60 min in order to melt the solid completely, followed by a rapid quenching into the liquid nitrogen. XRD experiments showed that the whole Se bar-shaped specimen with a diameter of 10 mm and a length of 50 mm is in an amorphous state. The as-quenched amorphous Se (a-Se) sample was annealed at 333 K for 400 h for a full structure relaxation. Then the a-Se sample, which was still kept in the vacuum ampoule, was heated up to the desired annealing temperature (ranging from 363 to 482 K) and held for 1.5 h so that the a-Se is completely crystallized. The crystallized Se sample was cooled from the annealing temperature down to room temperature at the rate of 0.2 K/min in order to minimize the microstrain. The resultant grain size of the as-crystallized Se was found to increase at higher annealing temperatures, ranging from 13 to 70 nm as determined from the XRD measurements. According to the Bragg reflection peak broadening in the XRD pattern, the mean grain size was calculated by consideration of the microstrain and the instrumental broadening effects. This grain-size result is verified by the transmission electron microscopy (TEM) observations of the as-crystallized Se samples. Table I lists the annealing conditions and the resultant grain sizes of the nc-Se specimens.

B. X-ray-diffraction measurements

The quantitative x-ray-diffraction measurements of the different grain-sized nc-Se samples were carried out on a Rigaku D/MAX 2400 x-ray diffractometer with a wide angle goniometer. The nc-Se sample used for XRD measurements was a flat sheet with a size of 15×9 mm^2 and a thickness of 4 mm, which was cut and polished from the nc-Se bar. A rotating Cu target was used with a voltage of 50 kV and a current of 100 mA. The x-ray wavelengths $\lambda_{k\alpha1}(=1.540\,562$ Å) and $\lambda_{k\alpha2}(=1.544\,39$ Å) were selected using a graphite crystal $\langle0002\rangle$ scattering at the goniometer receiving slit section. With these wavelengths, the extinction depth in Se was calculated to be less than 87 μm, which was much smaller than the thickness of the measured sample. The divergence slit (which was placed in the incident x-ray beam) was selected with a width of 0.5°, ensuring that the entire beam is either absorbed or diffracted by the sample. The scattering slit (which controls the scattering x-ray on the counter) was also chosen with a width of 0.5°. The width of 0.15 mm was selected as that of the receiving slit (which controls the width of diffracted x-ray to be entered into the counter). Measurements of θ–2θ scans for the samples were made in the reflection mode with the scattering vector aligned approximately perpendicular to the sample surface. The experimental temperature was 293 ± 1 K and the scan range for 2θ was 20°–103°. A small angular step of 2θ (0.02°) and a fixed counting time of 10 s were taken to measure the intensity of the Bragg reflections. For the rest of the XRD pattern, which is related to the background intensity, a step size of 0.1° and a counting time of 5 s were used.

C. Data analysis

Kinematical x-ray-diffraction theory was used to relate the measured intensity $I(\tau,T)$ as a function of scattering vector and temperature to the diffraction process $S(\tau)$ from the sample by[11]

$$I(\tau,T)=I_0LPA|f|^2\exp\left[\frac{-B(T)\tau^2}{8\pi}\right]S(\tau), \tag{1}$$

where I_0 represents the incident intensity multiplied by a set of physical constants, L and P are the Lorentzian and polarization factors respectively, A is the absorption factor and f is the atomic scattering factor. The physical constants within the I_0 term are independent of τ and T, which are not important in the present experiment because absolute intensities were not determined. The Lorentzian factor was taken to be equal to $(\sin^2\theta\cos\theta)^{-1}$. The polarization factor for the diffracted beam is given by

$$P(\theta,\alpha)=(1+\cos^2 2\alpha\,\cos^2 2\theta)/2, \tag{2}$$

where α is the Bragg angle of the monochromater that provides approximation as an ideal mosaic crystal. The absorption correction could be ignored for data collected with the scintillation detector because the samples were approximately flat. The atomic scattering factor f related to the scattering vector was taken equal to

$$f(\tau)=f_0+\Delta f'+(\Delta f'')^2/(2\,f_0+\Delta f''), \tag{3}$$

where f_0 is the atomic scattering magnitude of the free electrons, $\Delta f'$ and $\Delta f''$ are the dispersion correction terms. The term of $\exp[-B(T)\tau^2/8\pi^2]$ is the Debye-Waller factor, which accounts for the attenuation of intensity with the increasing angle. $B(T)$ is Debye-Waller parameter that is a measure of static and thermal displacements of atoms from their ideal lattice sites. $S(\tau)$ is the diffraction process that relates to the measured intensity of the sample.

In order to derive information about the Bragg shapes and the magnitude of the additional nonpeak intensity, the Pseudo-Voigt function was used to fit the data. The pseudo-Voigt function is a linear combination of Lorentzian and Gaussian functions represented by[12]

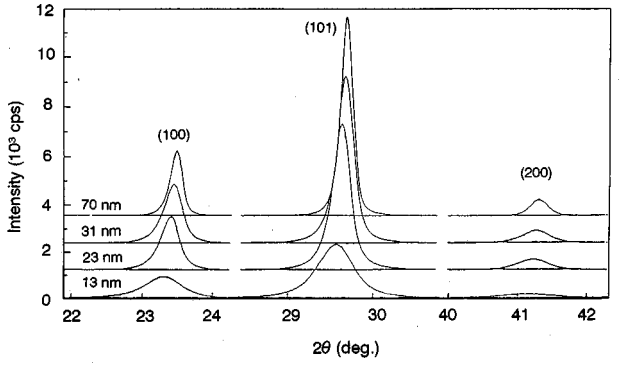

FIG. 1. The x-ray diffraction profiles of (100), (101), and (200) for the nc-Se samples with different grain sizes (as indicated).

$$\Phi_k(\tau)=\frac{2\eta_L\Psi_k}{\pi\Gamma_{kL}}\left[1+\frac{4(\tau-C_k)^2}{\Gamma_{kL}^2}\right]^{-1}+\frac{2(1-\eta_L)\Psi_k[(\ln 2)/\pi]^{1/2}}{\Gamma_{kL}}\times\exp\left[\frac{-4\ln 2(\tau-C_k)^2}{\Gamma_{kL}^2}\right]\quad(\tau<C_k),\qquad(4a)$$

$$\Phi_k(\tau)=\frac{2\eta_R\Psi_k}{\pi\Gamma_{kR}}\left[1+\frac{4(\tau-C_k)^2}{\Gamma_{kR}^2}\right]^{-1}+\frac{2(1-\eta_R)\Psi_k[(\ln 2)/\pi]^{1/2}}{\Gamma_{kR}}\times\exp\left[\frac{-4\ln 2(\tau-C_k)^2}{\Gamma_{kR}^2}\right]\quad(\tau>C_k),\qquad(4b)$$

where Ψ_k, Γ_k, and C_k are the integrated intensity, full width at half maximum, and centroid position of the kth intensity peak, respectively. The parameter η weights the relative amounts of Lorentzian and Gaussian components, such that $\eta=1$ is the pure Lorentzian and $\eta=0$ is the pure Gaussian.

The parameters η and Γ_k were adjusted independently and fitted in the peak profiles of the nonsubject. For each peak, when τ was in the left of the peak position C_k, Eq. (4a) was used to calculate the left side of the Bragg reflection, when τ was in the right of the peak position C_k, Eq. (4b) was used to present the right side shape.

III. RESULTS AND DISCUSSIONS

A. The integrated intensities of the Bragg reflections

Figure 1 shows typical XRD lines (100), (101), and (200) for the nc-Se bulk samples with different grain sizes. It is obvious that with a decrease of grain size, the Bragg diffraction lines are significantly broadened, and the peak positions C_k shift towards lower τ values (smaller 2θ values).

In order to separate the background intensity from the intensity of Bragg reflection that has been fitted by using the pseudo-Voigt analysis, a couple of edge points located at the both corners of each Bragg reflection were chosen as the background. So, the baseline connecting these edge points was established. The intensity data above the base line were removed for all Bragg reflections. The remained intensity

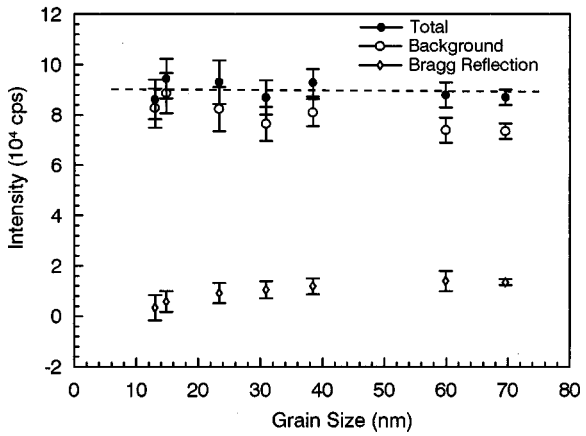

FIG. 2. Variations of the background integrated intensity (open circles), the integrated intensity of the Bragg reflections (open rhombuses), and the total scattered intensity (full circles) from $2\theta=20°$ to 103° with the mean grain size for the nc-Se specimens. The dashed line is obtained by the least-square fitting of the measured total scattered intensity.

that is not associated with the Bragg reflection is regarded as the background intensity. Figure 2 shows the integrated intensities of background and Bragg reflections from $2\theta=20°$ to 103° for the nc-Se samples. It is clear that with a decrease of grain size from 70 to 13 nm, the background intensity increases slightly from $(7.4\pm0.3)\times10^4$ to $(8.2\pm0.8)\times10^4$ cps (about $11\pm7\%$ enhancement), and the integrated intensity of Bragg reflections decreases from $(1.3\pm0.1)\times10^4$ to $(0.3\pm0.3)\times10^4$ cps. A roughly constant Bragg reflection intensity was observed for the nc-Se samples with grain sizes greater than 40 nm. The total scattered intensity of the nc-Se sample, which is a sum of the background and Bragg reflection intensities, keeps unchanged with grain size, as seen in Fig. 2.

Similar results were reported that an enhanced background intensity in the nc Pd (Ref. 13) (about $8\pm8\%$) and Cu (Ref. 6) ($6\pm3\%$), in comparison with those in the conventional coarse-grained counterparts. However, a very large intensity of background scattering was observed in a nc Fe (with a bcc structure), which was regarded as originating from a ''gaslike'' grain-boundary structure.[14] The present result seems to imply the so-called ''gas-like-structured'' grain boundaries with neither the short-range order nor the long-ranged order have not been detected at least in the present clean nc samples.

The background intensity in XRD patterns is a result of x-ray diffuse scattering from the samples and the instrument. In the present experiments, due to the same background intensity from the instrument, the background intensity from the nc-Se samples can be compared. The increased background intensity patterns indicates a larger x-ray diffuse scattering from the sample. This observation, as well as the decreased Bragg reflection intensity, might be attributed to larger atomic displacements from their equilibrium sites in the grains and on grain boundaries of which the volume fraction increases considerably with a reduction of grain size in the nanometer region.

B. The Bragg reflection shapes analysis

By using the Pseudo-Voigt function [Eqs. (4a) and (4b)] fitting, the Bragg reflection shapes of these nc-Se samples

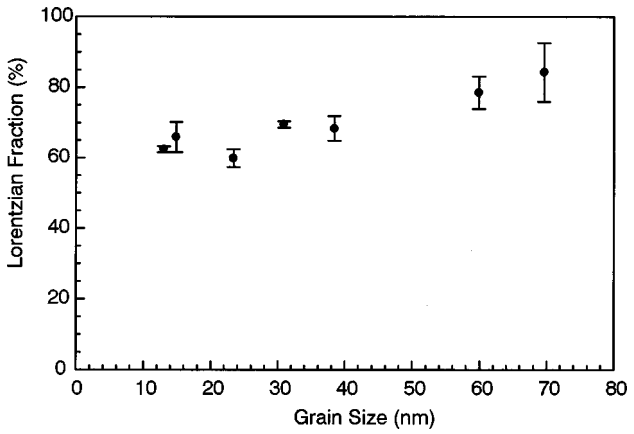

FIG. 3. Variation of the Lorentzian fraction for the Bragg reflections vs the mean grain size in the nc-Se samples.

can be described by means of a sum of Gaussian and Lorentzian functions with a larger Lorentzian component. For instance, the Lorentzian fraction is about $62\pm1\%$ (the Gaussian is $38\pm1\%$) for the nc Se with a mean grain size (D) of 13 nm. The Lorentzian component for the nc-Se sample was found to be decreasing with a reduction of grain size, from about $84\pm8\%$ (for $D=70$ nm) to $62\pm1\%$ ($D=13$ nm), as seen in Fig. 3. This variation tendency differs from the observations in the literature that enhanced Lorentzian components were detected in nc materials compared with their coarse-grained counterparts. It has been reported that in the nc Pd made by consolidation of UFPs,[4] the primary Lorentzian-shaped (more than 90% Lorentzian component) Bragg reflections were observed, in contrast to a 40–50% Lorentzian component in the coarse-grained polycrystalline Pd. A rather similar behavior has been found in Cu made by severe plastic deformation method.[6] The primarily Lorentzian shape of Bragg reflections in the nc samples was interpreted by the small crystallite size and the influence of the long-range internal stress fields of the nonequilibrium grain boundaries.[6]

The shape of the Bragg reflections is originated from the broadening profiles of the grain-size refinement, the microstrain, and the instrument. The grain-size broadening profile, which frequently dominates the reflection, can be normally represented by a pure Lorentzian function.[15] The microstrain broadening profile is related to the distribution of the microstrain in grains. According to the present results, the Lorentzian component varied with grain size, and the instrumental broadening profile (a Gaussian function) is the same for different nc-Se samples. Hence, it can be deduced that there exists a Gaussian component between grain size and microstrain broadening profiles. Considering that the grain-size broadening profile is a Lorentzian function, one may attribute the Gaussian component to the microstrain broadening. With a decrease of grain size, the Gaussian fraction gradually increases, indicating an increasing attitude of microstrain in the nc-Se specimens (as seen in Sec. III C).

C. Peak broadening effect analysis

The peak broadening is characterized by its integral width. The measured intensity profile of the Bragg reflection is a convolution of the physical intensity profile from the sample with a profile representing instrumental broadening. As shown above, the measured profile of the Bragg reflection in the nc-Se sample possesses primarily a Lorentzian component. The instrumental broadening profile determined by means of a SiO_2 reference sample is revealed as to be a Gaussian type in the present study. So, one can suppose that the physical profile of the nc Se is primarily a Lorentzian type. From the above analysis, one can separate the physical intensity profile from the measured intensity profile by removing the instrumental broadening effect. The microstructure broadening of the sample may originate from impurities, small crystallites, and the presence of microstrain within the specimen. As the effect of impurities can be ruled out for the pure nc-Se samples in this case, the physical broadening profile can be considered as the convolution of the grain-size broadening profile (usually represented by a Lorentzian function[4]) with that of the microstrain broadening (a Gaussian function as analyzed in Sec. III B).

According to the analyses above, the grain size and the microstrain of the sample can be calculated from the integral width of the physical broadening profile β in terms of the Scherrer and Wilson equation[16]

$$\frac{\beta_{hkl}^2}{tg^2\theta_{hkl}}=\frac{\lambda\beta_{hkl}}{D_{hkl}tg\,\theta_{hkl}\sin\theta_{hkl}}+4\langle\varepsilon_{hkl}^2\rangle^{1/2}, \tag{5}$$

where λ is the wavelength of $\lambda_{k\alpha_l}$, and D_{hkl} and $\langle\varepsilon_{hkl}^2\rangle^{1/2}$ represent the thickness and the mean magnitude of microstrain inside of the grains and the interfacial regions in the $\langle hkl\rangle$ direction, respectively.

Table II lists the resultant mean grain sizes and microstrains in the as-crystallized nc-Se samples calculated from

TABLE II. A list of the mean grain size and the mean microstrain, the grain sizes and microstrains along the $\langle100\rangle$ and $\langle104\rangle$ directions, and the grain boundary microstrain ($\langle\varepsilon^2\rangle_{gb}^{1/2}$) in the as-crystallized nc-Se samples.

Mean grain size, D (nm)	Mean microstrain, $\langle\varepsilon^2\rangle^{1/2}$ (%)	D_{100} (nm)	$\langle\varepsilon_{100}^2\rangle^{1/2}$ (%)	D_{104} (nm)	$\langle\varepsilon_{104}^2\rangle^{1/2}$ (%)	$\langle\varepsilon^2\rangle_{gb}^{1/2}$ (%)
13 ± 2	0.60 ± 0.08	15 ± 2	0.73 ± 0.07	10 ± 4	0.04 ± 0.07	1.1 ± 0.2
15 ± 1	0.39 ± 0.06	16 ± 1	0.51 ± 0.06	13 ± 3	0.06 ± 0.06	0.8 ± 0.1
23 ± 2	0.27 ± 0.02	31 ± 2	0.41 ± 0.05	20 ± 2	0.12 ± 0.04	0.7 ± 0.2
31 ± 3	0.29 ± 0.04	39 ± 3	0.43 ± 0.05	27 ± 3	0.13 ± 0.04	0.9 ± 0.1
38 ± 4	0.16 ± 0.05	43 ± 3	0.26 ± 0.04	35 ± 4	0.12 ± 0.05	0.7 ± 0.2
60 ± 6	0.20 ± 0.05	65 ± 5	0.23 ± 0.05	54 ± 5	0.13 ± 0.03	0.8 ± 0.2
70 ± 5	0.13 ± 0.01	77 ± 5	0.14 ± 0.02	65 ± 6	0.13 ± 0.02	

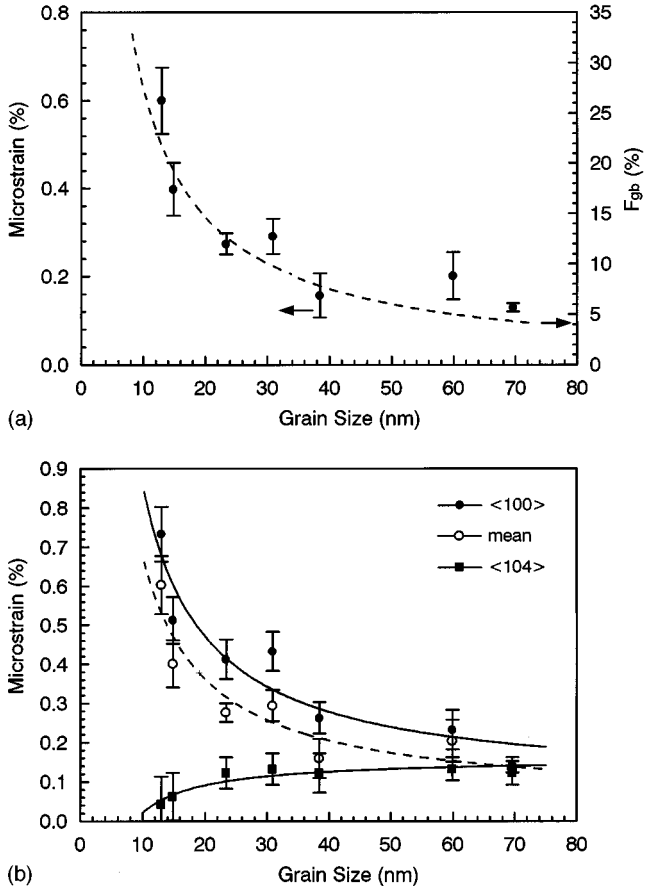

FIG. 4. (a) A plot of the mean microstrain vs the mean grain sizes in the nc Se. The dashed line represented the grain-size dependence of grain-boundary volume fraction (F_{gb}) in the nc sample. (b) A plot of the microstrains along ⟨100⟩ and ⟨104⟩ directions vs the mean grain size in the nc Se. The dashed line represents the variation of the mean microstrain with grain size.

nine single XRD peaks. Figure 4(a) shows the mean microstrains in the as-crystallized nc-Se specimens as a function of grain size. It is clearly seen that with a decrease of grain size (from 70 to 13 nm), the mean microstrain increases evidently from about 0.1% up to 0.6%. One can see from this result that the microstrains in the as-crystallized nc-Se samples are smaller compared to those in the mechanically-deformed nc materials [that reached as much as about 1–3 % (Refs. 17 and 18)]. The measured grain-size dependence of mean microstrain in the nc-Se sample has a similar tendency as that of the volume fraction of grain boundaries, $F_{gb}=3\delta/D$ (δ is the grain-boundary thickness), as indicated in Fig. 4(a), which is inversely proportional to the mean grain size. According to the two-state model,[5] one may describe the overall microstrain of a nc sample by $\langle\varepsilon^2\rangle_{nc}^{1/2}=F_{gb}\langle\varepsilon^2\rangle_{gb}^{1/2}+(1-F_{gb})\langle\varepsilon^2\rangle_c^{1/2}$, where $\langle\varepsilon^2\rangle_{gb}^{1/2}$ and $\langle\varepsilon^2\rangle_c^{1/2}$ are the microstrains for the grain boundary and the crystallite, respectively. Taking the mean microstrain of the 70 nm sample as $\langle\varepsilon^2\rangle_c^{1/2}$ ($=0.13\%$) for the crystallite and $\delta=2$ nm (a thickness of about four atomic layers), one can get $\langle\varepsilon^2\rangle_{gb}^{1/2}$, as shown in Table II. The $\langle\varepsilon^2\rangle_{gb}^{1/2}$ values seem to be independent of grain size, being a constant within the error bar, $\langle\varepsilon^2\rangle_{gb}^{1/2}=0.9\pm0.2\%$. The origin of the microstrain caused by the quenching can be ignored since the samples were cooled at a rather slow rate. Experiments also indicated that the microstrain does not change with the annealing time.[19] The observed variation of the mean microstrain might be attributed to larger atomic displacements from their equilibrium sites in the grains, and on grain boundaries of which the volume fraction increases remarkably with a decrease of grain size in the nanometer region.

Comparing Fig. 3 with Fig. 4(a), one can see that the inverse grain-size dependence of the mean microstrain is more pronounced than the variation of the Gaussian (or Lorentzian) component. As analyzed in Sec. III B, the shape of the Bragg reflections originates from (i) the broadening profile of the grain refinement (Lorentzian function), (ii) the microstrain broadening profile (Gaussian function), and (iii) the instrumental broadening profile (Gaussian). The instrumental broadening profile can be excluded as it is the same for different nc-Se samples. A reduction of grain size increases the Lorentzian component and hence depresses the Gaussian. Meanwhile, with a reduction of grain size, the microstrain component increases, which leads to a larger Gaussian component. Therefore, the overall variation of the Lorentzian component cannot be comparable with that of the microstrain.

Due to the overlapping of the second-order reflection peaks in the XRD spectra, (210), (201), and (100) reflections were selected to estimate the grain size and the microstrain along ⟨100⟩ direction, D_{100}, $\langle\varepsilon_{100}^2\rangle^{1/2}$ by Eq. (5), and (104) and (102) lines for D_{104}, $\langle\varepsilon_{104}^2\rangle^{1/2}$. The results are presented in Table II and Fig. 4(b). It can be seen that, with a reduction of grain size from 70 to 13 nm, $\langle\varepsilon_{100}^2\rangle^{1/2}$ increases apparently from $0.14\pm0.02\%$ to $0.73\pm0.07\%$, while $\langle\varepsilon_{104}^2\rangle^{1/2}$ decreases from $0.13\pm0.02\%$ to $0.04\pm0.07\%$, which can be well correlated with the variations of the lattice parameters a and c with grain size, as discussed in Sec. III D. An increasing anisotropic microstrain behavior is clearly seen for the nc-Se samples with smaller grains. For the 70 nm Se sample, the microstrains are comparable along ⟨100⟩ and ⟨104⟩ directions, but for the 13 nm sample, $\langle\varepsilon_{100}^2\rangle^{1/2}$ is about one order of magnitude larger than $\langle\varepsilon_{104}^2\rangle^{1/2}$. The Voigt function method[20] was also used to calculate the grain sizes and the microstrains along ⟨100⟩ and ⟨104⟩ directions, and similar results were obtained.

Similar to the present results, Eastman and co-workers[4] reported the strain breadths are essentially isotropic in the coarse-grained sample Pd, but very anisotropic in the nc sample. The nc Cu made by means of the severe plastic deformation method was also found to be anisotropic.[6] The strains along ⟨100⟩ direction were found to be much larger than those along ⟨111⟩ direction and in nc, Pd, and Cu samples,[4,6] while in the nc-Se samples the strain along ⟨100⟩ direction is larger than that along ⟨104⟩. Such a difference in the microstrain can be attributed to different crystallographic symmetries.

D. Refinement of lattice parameters

Determination of the lattice parameters in nc Se includes two stages. First, the $\lambda_{k\alpha2}$ component was removed from the XRD profiles using the modified Rachinger method.[21,22] Second, the lattice parameters were calculated from the intensity peak centroid positions for the nc-Se specimens. The peak

positions were calibrated by the external standard method using a pure Si polycrystal in order to minimize the systemic error. The calibration function was observed as

$$\Delta 2\theta = \alpha + \beta \cos\theta + \gamma \sin\theta, \tag{6}$$

where α relates to 2θ-axis origin displacement, β relates to eccentricity between the sample and goniometer center axis, and γ relates to the sample flatness or absorption. In this study, α, β, and γ were determined by the least-square method, being $\alpha = 0.013\,891$, $\beta = -0.080\,571\,2$, and $\gamma = 0.023\,696\,9$. Considering that the nc Se is the hexagonal structure, we select the weighted least-square method to calculate the lattice parameters in order to minimize the calculation error. The equation is originated from the Bragg's law and given by

$$h^2 \frac{a^*}{2} + k^2 \frac{b^*}{2} + l^2 \frac{c^*}{2} + 2kl \frac{b^*c^*}{\cos\alpha^*} + 2lh \frac{a^*c^*}{\cos\beta^*} + 2hk \frac{a^*b^*}{\cos\gamma^*} + E(\theta)x = \frac{4\sin^2\theta}{\lambda^2}, \tag{7}$$

where a^*, b^*, c^* and α^*, β^*, γ^* are the reciprocal-lattice parameters from which the lattice parameters of the nc Se can be obtained. $E(\theta)$ is the error function that is selected as $\sin^2 2\theta$ and x is the error function weight. Nine single peaks were used in the calculation.

Measured lattice parameters (a and c) for the nc-Se samples with different grain sizes are shown in Figs. 5(a) and 5(b). The values of a are evidently above the equilibrium lattice parameter a_0 ($=4.3662$ Å) with grain sizes smaller than 30 nm, for the nc Se with grain size larger than 35 nm, a values are approximately equal to a_0. The value of a is found to increase significantly with a reduction of grain size. The values of c are found to be larger (about 0.1–0.2 %) than the tabulated value of the equilibrium Se, c_0 ($=4.9536$ Å), and show a slight decreasing tendency with a reduction of grain size. The enhancement of the lattice parameter a with respect to a_0, $\Delta a = (a - a_0)/a_0$, increases from -0.05 to 0.3% when the grain size decreases from 70 to 13 nm. From Fig. 4(b), one can see that, with a reduction of the mean grain size, the microstrain along $\langle 100 \rangle$ direction (a axis) increases, but decreases along $\langle 104 \rangle$ direction (that can be regarded as c axis approximately). This behavior can be correlated with the variations of the lattice parameters a and c with grain size. However, the intrinsic nature of the different grain-size dependencies of the two lattice parameters (a and c) is actually unknown and needs further investigation.

The lattice parameters for the nc-Se samples from the XRD experiments may be considered as an weighted average from the atoms inside the crystallites and those on grain boundaries that satisfy the Bragg reflection conditions. Or, in other words, some of the atoms on the grain boundary may contribute to the Bragg reflection when they are associated with the crystallite lattice. The evident deviation of the measured lattice parameters of the nc-Se samples from the tabulated values for the equilibrium crystal implies (i) a lattice distortion in the crystallites, or (ii) a significant distortion localized in the grain boundaries while the crystallite lattice structure remains unchanged, or (iii) a distortion in both the crystallite and the grain boundaries. From the present available data, however, it is difficult to identify which situation holds in the nc-Se samples. Variation of the lattice parameters in trigonal nanophases has been observed in Ni_3P, Fe_2B,[23,24] in which the lattice parameter a is enhanced while c is depressed. In a cubic-structured nanophase (Cr, Pd),[25] increased lattice parameters were also reported based on the XRD measurements.

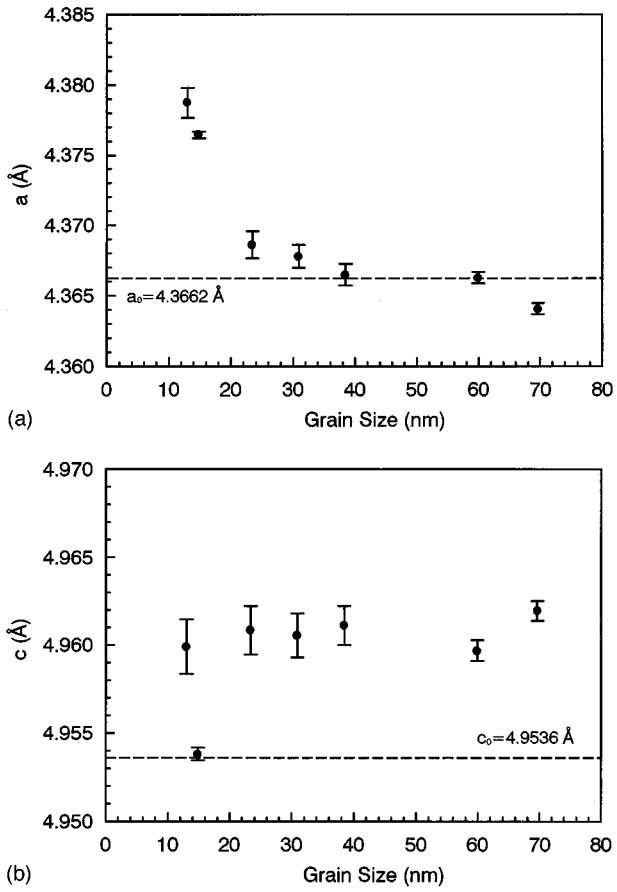

FIG. 5. (a) A plot of the measured lattice parameter a vs the mean grain size in the nc-Se samples. (b) A plot of the measured lattice parameter c vs the mean grain size in the nc-Se samples.

With the measured a and c, the unit-cell volume (V) of the nc-Se sample can be calculated according to $V = (\sqrt{3}/2)a^2c$. V is found to be larger than the equilibrium data (V_0) for all nc-Se samples, implying an evident lattice expansion in the nc Se. Figure 6(a) shows the variation of the unit-cell volume for the nc-Se specimens against the grain size. ΔV increases from around 0.1% to 0.7% with a reduction of grain size from 70 to 13 nm. The increased unit-cell volume is found to be proportional to D^{-1}, as shown in Fig. 6(b), which is similar to that observed in the nc Ni_3P, Fe_2B.[23,24]

From a thermodynamic point of view, the metastable structure with an enhanced unit-cell volume (or referred to as an effective lattice expansion) might be explained. With respect to that of the infinite large crystal, the free energy of a crystallite of which the dimension is D will be enhanced by $\Delta G(T,D) = 4\Omega\gamma/D$, where Ω is the atomic volume of the grain and γ is the interfacial free energy. From this point of view, a reduction of grain size will enlarge the free energy of

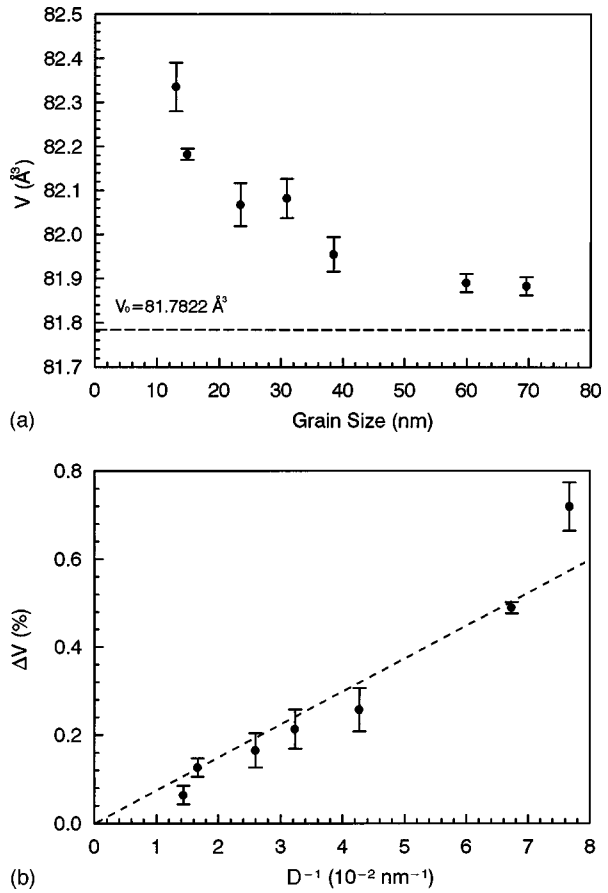

FIG. 6. (a) Variation of the unit cell volume V with the mean grain size in the nc Se. (b) A plot of the unit cell volume change $(\Delta V=(V-V_0)/V_0)$ with D^{-1}.

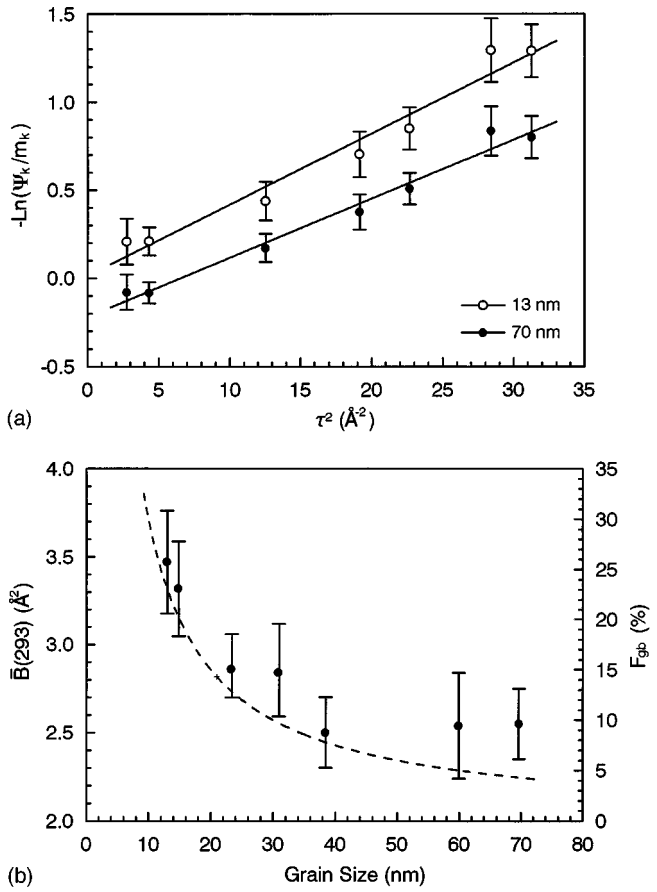

FIG. 7. (a) The logarithm of integrated peak intensities divided by the appropriate multiplicity factors and Lorentzian, polarization factors, structural factor for the nc-Se samples with the mean grain size of 13 and 70 nm. The straight lines represent the best weighted linear fit to the data. (b) Variation of the average Debye-Waller parameters with the mean grain size for the nc Se. The dashed line represented the grain-size dependence of grain-boundary volume fraction (F_{gb}) in the nc samples. The average Debye-Waller parameter for the equilibrium coarse-grained polycrystal Se [$\bar{B}^c(293)=2.35$ Å^2] is also indicated.

the crystallites and consequently raise the equilibrium solute solubility in the crystal lattice. In a pure element system, point defects and vacancies are possibly ''solute''. Introduction of more point defects or vacancies in the crystal lattice would disturb the lattice structure resulting in lattice distortion with a dilated unit cell.[26]

E. Debye-Waller parameter determination

The Debye-Waller parameter is a measure of the displacements of atoms from their ideal positions. Usually the Debye-Waller parameter can be obtained from XRD patterns by means of the Warren[11] method or other methods.[27,28] According to Eq. (1), the Warren method can be expressed as[11]

$$-\ln(\Psi_k/m_k)=\frac{-B(T)C_k^2}{8\pi^2}+J, \tag{8}$$

where Ψ_k is the integrated intensity, C_k is the centroid peak position, and m_k is the multiplicity factor of the kth intensity peak. The parameter J is a constant scaled with the incident intensity. Figure 7(a) shows plots of $-\ln(\Psi_k/m_k)$ vs τ^2 ($\tau=4\pi\sin\theta_{hkl}/\lambda$) for the nc-Se samples with grain sizes of 13 and 70 nm. It was observed that the plots are best fitted by straight lines, the average Debye-Waller parameters at room temperature (293 K), $B(293)$, can be obtained from the slope of the straight line. The obtained value of $B(293)$ for 13 nm Se [(3.5 ± 0.3) Å^2] is about 35% larger than that for 70 nm Se [(2.6 ± 0.2) Å^2]. These values for nc-Se specimens are obviously larger than that for the conventional coarse-grained polycrystalline Se (2.35 Å^2).[29] The average Debye-Waller parameter of the nc-Se specimen was found to increase with a reduction of grain size, as can be seen in Fig. 7(b). The grain-size dependence of the Debye-Waller parameter in the nc Se is consistent with previous observations in nc metals [Pd (Ref. 30), Au (Ref. 27), and Cu (Ref. 6)] in which enhanced $B(T)$ was detected relative to their coarse-grained counterparts. From a thermodynamic point of view as mentioned above, the variation of the Debye-Waller parameter of the nc-Se specimens against the grain size can be explained, since the increase in the free energy of the system due to the reduction of grain size is offset by enhanced solubility of defects that is measured by $B(293)$.

The determined Debye-Waller parameter according to Eq. (8) provides a measure of the atomic displacements from their ideal lattice sites averaged over all crystallographic orientations and regions. It may be separated into two components: B_T and B_S. B_T is the contribution from thermal vibration of atoms and is temperature-dependent. B_S is the

temperature-independent term due to the existence of the static lattice distortion, i.e., the static atomic displacements.[31] The present result indicated that the enhanced atomic displacements (thermal and static) in the grains and/or in the interfacial regions might take place in nc-Se samples. However, with these data, one cannot separate the contributions of the thermal motion and of the static atomic displacements. Nevertheless, based on the measurement results of microstrains and the lattice parameters for the nc Se with different grain sizes described in Secs. III C and III D, we may suppose that static atomic displacements might play an important role in the variation of $B(293)$. In order to identify the contributions of B_T and B_S to the observed enhancement of $B(293)$, it is necessary to measure the Debye-Waller parameters at different temperatures. With the temperature dependence of $B(T)$, B_T, and B_S could be separated and the origin of the $B(293)$ enhancement can be clarified, which will be discussed in our forthcoming paper.[10]

IV. CONCLUSIONS

Porosity-free bulk nanocrystalline element selenium samples with grain sizes ranging from 13 to 70 nm made by nanocrystallization of melt-quenched amorphous Se have been investigated by means of quantitative XRD analysis. The Bragg reflections of the nc-Se specimens can be represented by a sum of Gaussian and Lorentzian functions with a larger Lorentzian component. With a reduction of grain size, the Lorentzian component of the Bragg reflection shapes decreases, and the background integrated intensity of the XRD pattern increases. When the grain size decreases from 70 to 13 nm, the mean microstrain in the nc Se was found to increase from about 0.1% to 0.6%, and the microstrain increases significantly along the ⟨100⟩ direction but decreases along the ⟨104⟩ direction, exhibiting an increasing anisotropic microstrain behavior.

The lattice parameters and the Debye-Waller parameter for the nc-Se specimens were found to be strongly dependent on the grain size. An evident lattice distortion was observed with an enhanced unit-cell volume relative to the equilibrium lattice structure. With a reduction of grain size, a increases significantly by as much as about 0.3%, but c decreases slightly, the unit-cell volume increases by about 0.7% with $D=13$ nm. The distorted lattice structure with a dilated unit-cell volume is consistent with the grain-size dependence of the average Debye-Waller parameter that increases with a reduction of grain size, suggesting larger atomic displacements in the nc Se with smaller grains.

The observed grain-size dependencies of microstrain, unit-cell volume, and the Debye-Waller parameter in the nc-Se samples exhibit approximately D^{-1} relations, and are rather consistent with that of the volume fraction of grain boundaries in nc materials. The results imply that the intrinsic microstructure feature of nc materials is closely related to the crystallite dimension and the amount of grain boundaries.

ACKNOWLEDGMENTS

This work was financially supported by the National Science Foundation of China (Grant Nos. 59625101 and 59431021) and the Chinese Academy of Sciences.

*Corresponding author. Fax: +86-24-3891 320; Tel: +86-24-3843 531; Electronic address: kelu@imr.ac.cn

[1] H. Gleiter, Prog. Mater. Sci. **33**, 223 (1989).
[2] C. Suryanarayana, Int. Mater. Rev. **40**, 41 (1995).
[3] R. W. Siegel, in *Physics of New Materials 27*, edited by F. E. Fujita (Springer, Berlin, 1994), p. 65.
[4] J. A. Eastman, M. R. Fitzsimmons, and L. J. Thompson, Philos. Mag. B **66**, 667 (1992).
[5] J. A. Eastman and M. R. Fitzsimmons, J. Appl. Phys. **77**, 522 (1995).
[6] K. Zhang, I. V. Alexandrov, R. Z. Valiev, and K. Lu, J. Appl. Phys. **88**, 5617 (1996).
[7] R. Z. Valiev, A. V. Korznikov, and R. R. Mulykov, Mater. Sci. Eng. A **168**, 141 (1993).
[8] K. Lu, J. T. Wang, and W. D. Wei, J. Appl. Phys. **69**, 522 (1991); Scr. Metall. Mater. **24**, 2319 (1990).
[9] K. Lu, Mater. Sci. Eng. R. Rep. **R16**, 161 (1996).
[10] Y. H. Zhao and K. Lu, following paper, Phys. Rev. B **56**, 14 330 (1997).
[11] B. E. Warren, *X-ray Diffraction*, (Dover, New York, 1990), p. 251.
[12] D. E. Cox, J. B. Hastings, L. P. Cardoso, and L. W. Finger, Mater. Sci. Forum **9**, 1 (1986).
[13] M. R. Fitzsimmons, J. A. Eastman, M. Muller-Stach, and G. Waller, Phys. Rev. B **44**, 2452 (1991).
[14] X. Zhu, R. Birringer, U. Herr, and H. Gleiter, Phys. Rev. B **35**, 9085 (1987).
[15] J. I. Langford, R. Delhez, Th. H. de Keijser, and E. J. Mittemeijer, Aust. J. Phys. **41**, 173 (1988).
[16] H. P. Klug and L. E. Alexander, *X-ray Diffraction Procedures for Polycrystalline and Amorphous Materials*, 2nd ed. (Wiley, New York, 1974), p. 662.
[17] E. Hellstern, H. J. Fecht, Z. Fu, and W. L. Johnson, J. Appl. Phys. **65**, 305 (1989).
[18] G. W. Nieman, J. R. Weertman, and R. W. Siegel, Mater. Res. Soc. Symp. Proc. **206**, 493 (1991).
[19] Y. H. Zhao and K. Lu (unpublished).
[20] J. I. Langford, J. Appl. Crystallogr. **11**, 10 (1978).
[21] J. Labell, A. Zagofsky, and S. Pearman, J. Appl. Crystallogr. **8**, 499 (1975).
[22] G. Platbrood, J. Appl. Crystallogr. **16**, 24 (1983).
[23] M. L. Sui and K. Lu, Mater. Sci. Eng. A **179-180**, 541 (1994).
[24] X. D. Liu, K. Lu, B. Z. Ding, and Z. Q. Hu, Nanostruct. Mater. **2**, 581 (1993).
[25] J. A. Eastman, M. R. Fitzsimmons, L. J. Thompson, and A. C. Lawson, Nanostruct. Mater. **1**, 465 (1993).
[26] K. Lu and M. L. Sui, J. Mater. Sci. Technol. **9**, 419 (1993).
[27] J. Harada, S. Yao, and A. Ichimiza, J. Phys. Soc. Jpn. **48**, 1625 (1980).
[28] S. S. Lu and J. K. Liang, Acta Phys. Sin. **30**, 1361 (1981).
[29] *International Tables for X-ray Crystallography III*, edited by C. H. Macgillavry and G. D. Rieck (Reidel, Dordrecht, 1983), p. 239.
[30] K. Ohshima, S. Yatsuya, and J. Harada, J. Phys. Soc. Jpn. **50**, 3071 (1981).
[31] M. A. Krivoglaz, *Theory of X-ray and Thermal-Neutron Scattering by Real Crystals* (Plenum, New York, 1969).